Article

Screening of Low-Dosage Methanol as a Hydrate Promoter

Jyoti Shanker Pandey * , Saad Khan and Nicolas von Solms *

Center for Energy Resource Engineering (CERE), Department of Chemical Engineering, Technical University of Denmark, 2800 Kongens Lyngby, Denmark

* Correspondence: jyshp@kt.dtu.dk (J.S.P.); nvs@kt.dtu.dk (N.v.S.)

Abstract: We report a quantitative study of the effect of low-concentration methanol (MeOH) on the formation and dissociation of hydrates based on CH_4 and CO_2/N_2 guest molecules. The kinetic promotion and dissociation ability of MeOH is also compared with the anionic surfactant sodium dodecyl sulfate (SDS, 100 ppm, 50 ppm). The effects of concentration changes (1 wt% and 5 wt%), pressure (p = 80–120 bar), guest molecules (CH_4 and CO_2), and temperature (1 °C and below 0 °C) are investigated using slow constant ramp (SCR) and isothermal (IT) temperature schemes. The results show that the kinetics are affected by the guest molecule and MeOH concentration. For CH_4 gas, 5 wt% MeOH shows better promotion, while for CO_2/N_2 gas mixtures, 1 wt% MeOH gives better promotion. This conclusion agrees well with our previous results demonstrating optimal CH_4 recovery and CO_2 storage in the presence of 5 wt% MeOH. The promoting and inhibiting properties of MeOH could be beneficial in CH_4 production from gas hydrate using CO_2-rich gas injection, as delayed hydrate film formation in the presence of MeOH could improve both CH_4 recovery and CO_2 storage.

Keywords: formation; dissociation; methanol; hydrate swapping; gas hydrate; CH_4 hydrate; CO_2 hydrate

1. Introduction

Methanol (MeOH) is commonly used in high doses as an antifreeze to prevent gas hydrate (GH) formation in oil and gas pipelines. GH formation blocks pipelines and can pose a safety risk and significant economic cost to operators in the upstream petroleum industry. In the presence of MeOH, the chemical potential of water decreases and the gas hydrate stability curve shifts to higher pressure and temperature conditions.

Recent studies show that MeOH in low concentrations (1 to 30 wt%) can enhance carbon sequestration and storage in high-pressure, low-temperature geological formations such as hydrate reservoirs [1–4]. There are two common studies on the storage of CO_2 in gas hydrates formed in geological formations in colder regions. In the first method, CO_2 is injected into CH_4 hydrates to enable hydrate exchange [5], and in the second method, flue gas is injected into water-saturated sediments in permafrost regions [4,6]. In both cases, the presence of additives is considered beneficial for altering pore water chemistry and thus controlling the kinetics of hydrate formation and dissociation.

For example, an enhanced exchange of CH_4-CO_2 hydrates is observed in the presence of 5 wt% MeOH. This is due to the role of MeOH as a kinetic inhibitor that can retard the formation of hydrates at low dosage. In the presence of MeOH, the thermodynamic driving force for the exchange between CH_4-CO_2 hydrates also increases [1]. In another study, MeOH showed a positive effect on CH_4-CO_2 exchange when used at 30 wt% compared to a salt such as NaCl [2]. MeOH is also miscible with water and lowers the freezing point of water, which is important for the injectivity of CO_2 in geological storage [3]. Recent laboratory studies confirm the promoting effect of MeOH on gas hydrate formation at low concentrations [7–9]. Molecular simulations show that the transport of CH_4 to the liquid phase is promoted due to the reduced interfacial free energy in the CH_4 and water system [10]. Other studies show that the promotion effect could result from the propagation

of the Trout–Buch defect [11] below 273 K, which enhances the stabilization of the hydrogen bonds of the molecules and thus accelerates the reaction rate. Further computational and spectroscopic studies suggest that MeOH forms gas hydrates with hydrophobic molecules such as ether [12]. Neutron diffraction experiments performed for a MeOH-water system at 200 K show the presence of a hexagonal ice structure and support the hypothesis that MeOH and water form amorphous co-deposits to accelerate hydrate formation when the gas and aqueous solution are under suitable pressure–temperature conditions [7,13]. FTIR experiments show the behavior of MeOH as a co-guest molecule and its ability to form strong hydrogen bonds with the water cage molecules [12].

Gas hydrate-based industrial processes such as gas storage and transport, gas separation, gas production, and desalination [14–18] depend on enhanced mass transfer at the gas–liquid interface, leading to improved water-to-gas conversion and faster kinetics. During formation, the hydrate film at the gas–liquid interface acts as a diffusion-based mass-transfer barrier, keeping gas molecules out of the liquid phase. Mechanical techniques such as agitation [19] and spraying through nozzles [20] improve the formation and growth process but increase energy consumption and maintenance requirements. Therefore, scientific research is focused on making the process simple, energy efficient, environmentally friendly, and cost-effective. In this context, the application and synthesis of chemical additives are of particular interest. The presence of chemicals enhances mass transfer from gas molecules to the liquid phase through various mechanisms, such as the solubilization of gas molecules and diffusion into the liquid phase, retardation of hydrate film formation at the gas–liquid interface, or alteration of hydrate morphology at the interface or throughout the system. Chemicals such as surfactants and hydrophobic amino acids, also known as kinetic promoters, shorten the formation time, increase the formation rate, and improve gas capture [21–24]. Thermodynamic promoters are used to achieve moderate operating conditions during hydrate formation, but achieve lower gas uptake compared to kinetic promoters [25].

The anionic surfactant sodium dodecyl sulfate (SDS) is the most effective known promoter for promoting hydrate formation. It has been studied for various gas hydrates, including CH_4, CO_2, CH_4/CO_2, and CO_2/N_2 mixtures. Parameters such as the Krafft point and critical micelle concentration (CMC) are used to explain properties such as surfactant solubility and surface tension effects [26]. Above the temperature of the Krafft point, the solubility of the surfactant increases sharply. At the Krafft point, the solubility of the surfactant is equal to the CMC [22]. The role of SDS in promoting gas hydrate formation is discussed in terms of CMC, since no change in the Krafft point is observed under hydrate formation conditions [27]. A change in adsorption and surface tension behavior is observed at a CMC of SDS [28]. On the other hand, the effect of MeOH at low dosage on the kinetics of formation and dissociation is not well-studied.

The kinetics of hydrate formation and dissociation are usually studied in terms of parameters such as onset temperature, induction time, and gas uptake, often using a high-pressure cell apparatus at low temperatures. The studies show that the kinetic studies are system-dependent. The kinetics of formation and dissociation in a bulk medium and a porous medium also differ due to factors such as the difference in gas–liquid interface and the difference in thermal conductivity of the system, etc. Kinetics in bulk media is usually studied using spectroscopic techniques such as Raman, NMR, and high-pressure reactors, while kinetics in porous media has been studied using micromodels, X-rays CT, magnetic resonance imaging (MRI), and high-pressure core flooding systems with confining pressures [29]. Due to differences in P and T conditions and differences in the high-pressure apparatus, experimental techniques, and sample preparation, kinetic results are poorly reproducible. A rocking cell offers advantages over high-pressure vessels, including stirred/unstirred reactors, autoclaves, and fixed-bed chambers, because the sample size is small, the experiments are standardized, and multiple parallel experiments can be performed at similar temperature conditions, which shortens the experimental

time [30,31]. It is common to test the performance of hydrate inhibitors, and recently low-dose hydrate promoters have also been tested in rocking cells [21,22].

In this study, we investigate the formation and dissociation kinetics of CH_4 hydrate and CO_2/N_2 hydrates (using 20 mol% CO_2 in CO_2/N_2) in the presence of MeOH (at low concentration in aqueous solution) using a rocking cell. The effects of concentration (1 wt% and 5 wt%) and pressure (60–120 bar) are studied with slow constant ramps and isothermal temperature schemes. Key parameters and behaviors studied include the onset temperature, dissociation temperature, dissociation behavior below 0 °C, induction time, total gas uptake, and CO_2 separation efficiency; a related discussion is also included.

2. Materials and Methods

2.1. Setup and Materials

An analytical grade CH_4 gas and CO_2/N_2 cylinder with 99.99% purity was obtained from Air Liquide. Chemicals, such as Methanol (MeOH) and anionic surfactant sodium dodecyl sulfate (SDS) with a certified purity of >99%, were purchased from Sigma Aldrich. All chemicals were used without any further purification. Deionized water was produced in our lab with a resistivity of 17 mΩ cm^{-1}.

A rocking cell setup with five identical high-pressure test cells (RC-5, PSL Systemtechnik, and Germany) was used. The RC-5 rocking cell has five stainless cells submerged into single liquid bath. Therefore, all cells experienced a similar temperature at the same time (refer to Figure 1). The RC-5 bath system can operate up to 200 bar and −10 °C to 60 °C temperature range. P, T, and temperature reading can be observed built into the data logging system. MeOH concentrations used were 1 wt% (abbreviation as MeOH-A) and 5 wt% (abbreviation as MeOH-B), whereas SDS concentrations were 50 ppm (abbreviation as SDS-A) and 100 ppm (abbreviation as SDS-B). Temperature sensors have accuracy in the range of $\pm$0.2 °C, and pressure sensors have accuracy in the range of 0.1% [32]. The combined setup uncertainty for the experiments using Stephanie Bell's methodology was calculated to be less than 1% [33]. A detailed setup discussion is also provided in our previous papers [34,35]. Rocking cell provides additional advantages such as the standardization of test, ability to test at high pressure (up to 200 bars), multiple testing at once, and long-duration stable experiments with accurate measurement that matches with simulation [36]. Distilled water was used to prepare all the samples to minimize the influence of impurities in the solution phase.
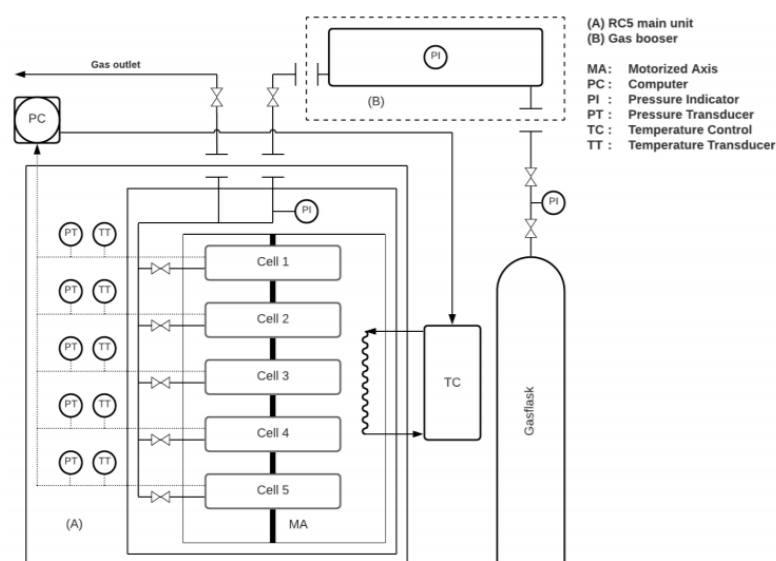

Figure 1. Schematic of rocking cell setup procured from PSL Systemtechnik, Germany.

2.2. Methods

A rocking cell setup with five identical pressure rigs (RC-5, PSL Systemtechnik, and Germany) was used to measure the pressure–time curve in the presence of MeOH, SDS, and different gases during hydrate formation and dissociation. Slow constant ramping (SCR) and isothermal temperature schemes were used. Pressure in the experiment varied between 60 and 120 bar. The temperature during slow constant ramping experiment changed from 15 °C to −1 °C in 14 h, while in isothermal it remained constant at 1 °C. SCR was used to identify the onset temperature (T_o) and dissociation temperature (T_d). Isothermal temperature scheme was used to identify the induction time (t_o) and methane gas uptake (n_{CH4}) for different operating pressure and chemicals. Measurement during constant ramping has shorter deviation and better reproducibility compared with isothermal testing [37].

For each cell, the volume was 40.13 cm^3, and the sample volume was 10 cm^3. The Rocking rate and rocking angle was 20 rocks/min and 35°, respectively. Parameters associated with setups such as rocking angle, rocking frequency, solution volume, rocking ball material type, and operating conditions on rocking cell performance have been studied extensively [37]. The setup was connected to a data acquisition system to record the variation. For isothermal experiments, two repetitions per experiment were performed and reported values were averaged.

2.3. Experimental Data Processing

During the SCR temperature scheme, when the system is outside the hydrate-stability zone, the pressure change depends on the methane solubility in water and the presence of a promoter. For a given promoter, as the temperature decreases, the solubility increases and thus the pressure decreases. Thus, there is a linear trend between pressure and temperature. However, in the hydrate-stability zone, gas solubility in water decreases in the presence of hydrate, and pressure has no effect on gas solubility [38,39]. Thus, pressure decreases due to gas consumption in hydrates without any significant contribution from gas solubility. The onset temperature T_o is the temperature at which hydrate nucleation begins and is identified as the point at which pressure deviates from a linear curve. The onset temperature is also the temperature below which rapid hydrate formation occurs, and the effect of chemicals on hydrate growth becomes negligible [40]. Due to the lack of transparent observation windows in the current experimental setup, it is not possible to visually confirm hydrate formation, and hydrate nucleation may have occurred above the value determined by the experimental setup.

Sub-cooling temperature (ΔT_{sub}) during SCR is the difference between T_{eq} and operational temperature T_o [41]. To is the nucleation temperature (onset temperature) observed at the start of the nucleation. T_{eq} for a given gas molecule is calculated using CSMGem software. CSMGem software is based on Gibbs energy minimization concept, and more details can be referred to in this article [42]. T_{op} is the operating temperature mostly referred to as the temperature during the isothermal test [21,43–45]. Subcooling measurement explains the effect of concentration on driving force and growth profile. It can be calculated as

$$\Delta T_{sub,cons} = T_{eq} - T_o \tag{1}$$

For Isothermal test, subcooling requirement is given by the equation below:

$$\Delta T_{sub,iso} = T_{eq} - T_{op} \tag{2}$$

$\Delta T_{sub,cons} - \Delta T_{sub,iso}$ gives the difference between the operating temperature (isothermal tests) and the expected onset temperature [46]. It is calculated by

$$\Delta T_{sub,cons} - \Delta T_{sub,iso} = (T_{eq} - T_o) - (T_{eq} - T_{op}) = T_{op} - T_o \tag{3}$$

$T_o > T_{op}$ indicates immediate hydrate formation, while $T_o < T_{op}$ indicates delayed hydrate formation. In general, in isothermal tests, operating temperature is always consid-

ered lower than the onset temperature. Previously, studies have shown that $T_o > T_{op}$ when $1 < T_{op} < 4\,°C$ [21,22].

To study the induction time and total gas uptake, isothermal experiments are performed at $1\,°C$ and in the presence of MeOH (1 and 5 wt%) and SDS (50 and 100 ppm). The pressure difference between the initial operating pressure Pi and the stability pressure Peq serves as the driving force during the isothermal experiment. Peq is calculated for a given isothermal temperature using CSMGem software. Increasing the initial operating pressure at constant temperature increases the driving force. In this study, isothermal experiments were performed for both CH_4 gas hydrate and CO_2/N_2 gas hydrate. The pressure variations during the isothermal temperature scheme were also used to calculate the gas uptake, as explained below. The gas uptake calculations were similar to our recent articles using a rocking cell setup [21,22]. The sample volume used in our study was 10 mL with additive. Completion of formation is indicated by the flat pressure line versus time and at constant temperature. Constant ramp and isothermal experiments were repeated without interruption, and repeated runs are referred to as storage runs, because the sample was exposed to the formation and dissociation cycle in the first cycle. In isothermal experiments, the temperature was kept constant at $1\,°C$ for 14 h, followed by 3 h in which the temperature increased rapidly from $1\,°C$ to $25\,°C$ to $1\,°C$ before the memory run started at $1\,°C$ (for the next 14 h). The temperature was lowered from $1\,°C$ to $-2\,°C/-4\,°C$ in one hour and held at $0\,°C$ for the next 24 h to study self-preservation. During the constant ramp experiments, the initial temperature was $25\,°C$. The system temperature moved from $25\,°C$ to $15\,°C$ in 2 h and from $15\,°C$ to $1\,°C$. The temperature dropped by $1°C$ in 1 h for a total of 14 h. The system temperature remained at $1\,°C$ for 5 h. Then, it increased from $1\,°C$ to $15\,°C$ in 14 h. No memory run was performed during the constant ramp operation.

3. Results

Isothermal and constant ramping temperature schemes are used to study the kinetics of formation and dissociation with respect to change in concentration and driving force. Key parameters observed during the study included the onset of nucleation temperature, induction time, nucleation temperature, and total gas uptake.

3.1. CH_4 Formation and Dissociation Kinetics

Rocking rigs are typically used to investigate inhibitors. Testing additives promotion capabilities is a relatively new practice [22]. Inhibitors testing involves multiple repetitions due to its enhanced stochastic nature. Due to its enhanced stochastic nature in the presence of inhibitors, multiple repetitions are required, whereas in the presence of promoters, the repetition requirement is less due to the reduced probabilistic nature. T_o values of promoters are often lower than those in pure water cases [21,22], suggesting nucleation in the presence of a promoter starts at a lower temperature compared with pure water. T_o is also affected by pressure and concentration change, as well as the difference in chemical structure and properties.

3.1.1. Onset Temperature (T_o) and Subcooling ΔT_{sub} for CH_4 Hydrate

The average onset temperature T_o for MeOH and SDS is summarized in Table 1. The pressure response curve during the SCR scheme is illustrated in Figure 2. $T_{eq} = 10.92\,°C$ for $p = 80$ bar for the H_2O-CH_4 system. T_o is recorded for both fresh and memory runs. The subcooling requirement for nucleation to start is also calculated.

Experimental observation confirms $T_o < T_{eq}$ in the presence of MeOH and SDS. Lower T_o indicates delayed nucleation and a higher subcooling requirement for methane hydrate in the presence of SDS and MeOH. For MeOH, T_o decreases from $9.1\,°C$ to $6.4\,°C$ when concentration increases from 1 wt% to 5 wt%, whereas for SDS, T_o increases from 8.4 to $8.8\,°C$ when concentration increases from 50 ppm to 100 ppm. Maximum $T_o = 9.65\,°C$ recorded for pure water case, lower than P_{eq} of the bulk water-CH_4 system. In Figure 2, a rapid pressure drop is visibly observed for SDS 100 ppm, followed by MeOH 5 wt%

concentration at 80 bar. For the rest of the chemicals, including water, no significant rapid pressure drop is observed.

Table 1. Averaged onset nucleation temperature T_o (°C) and subcooling (ΔT_{sub}) for CH_4 hydrate in the presence of MeOH and SDS (T_{eq} for CH_4 hydrate = 10.92 °C).

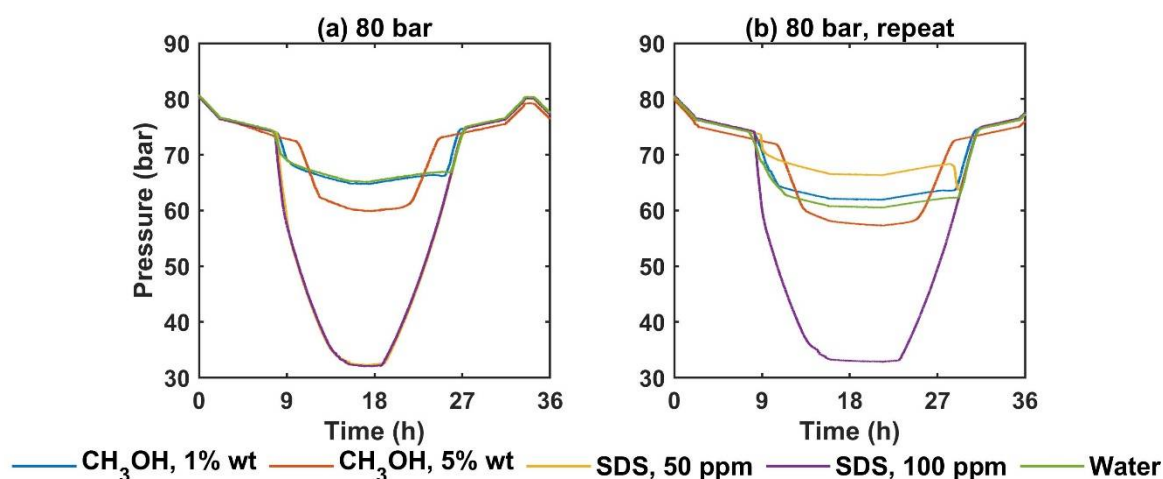|	**CH$_4$**			
80 bar	**Fresh**		**Memory**	
	T_o (°C)	ΔT_{sub} (°C)	T_o (°C)	ΔT_{sub} (°C)
MeOH-A	9.1	1.82	9.0	1.92
MeOH-B	6.4	4.52	6.3	4.62
SDS-A	8.4	2.52	8.6	2.32
SDS-B	8.8	2.12	8.8	2.12
Water	9.7	1.27	9.7	1.27

Figure 2. Pressure profiles during the constant ramping temperature scheme in the presence of MeOH (1% wt, 5 wt%) and SDS (50 ppm, 100 ppm). Starting pressure 80 bar and starting temperature 25 °C, and final temperature 1 °C. Temperature ramping rate 1 °C/h between 15 °C–1 °C. (**a**) starting pressure 80 bar fresh run; (**b**) 80 bar fresh and repeat.

No rapid pressure drop is observed for the other chemicals, including water. Figure 3 shows the data from Table 1. Of all the chemicals tested, at a given pressure *p* = 80 bar, the maximum subcooling is required for MeOH (5 wt%) and the least subcooling is required for water. The average To of SDS is higher than that of MeOH-B and similar to that of MeOH-A. In a previous study, the To for CH_4 hydrate in the presence of SDS (500–3000 ppm) was found to be between 7.9 and 8.1 °C at 70 bar and 9.2 and 10.5 °C at 90 bar [22]. This suggests that increasing the concentration of SDS has no significant effect on the onset of temperature To. It is also suggested that the effect of concentration on To becomes more pronounced at a higher initial pressure. Although MeOH-A has a higher To value compared to MeOH-B, a larger pressure drop is recorded in the presence of MeOH-B than MeOH-A.

3.1.2. The Onset of Dissociation Temperature (T_d) for CH_4 Hydrate

Table 2 contains averaged T_d values (for two new runs) for CH_4 dissociation during the SCR experiment. T_d is characterized by the end of the rapid pressure rise and the beginning of the linear relationship between pressure and temperature. The temperature ramp with a rate of 1°C/h between 1–15 °C is used to determine T_d.
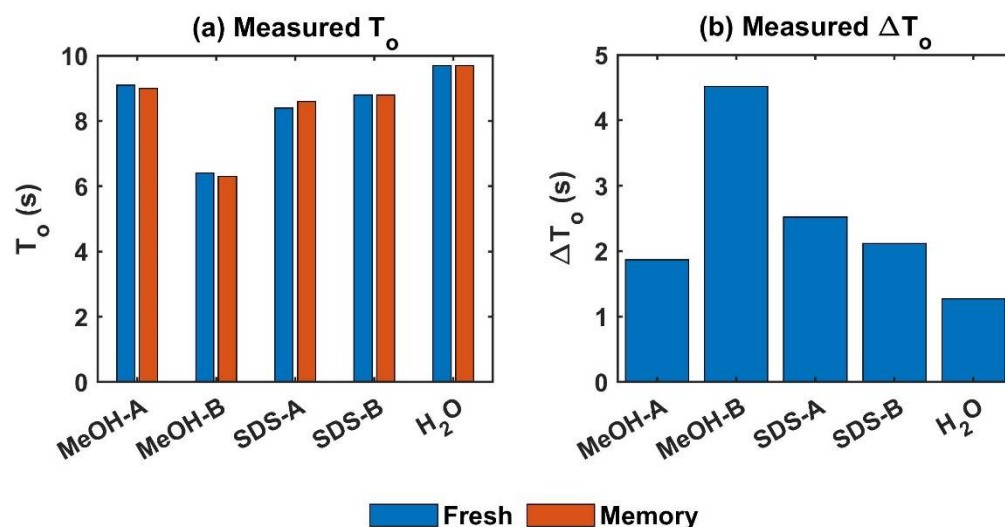
Figure 3. To and subcooling measurements for MeOH (1 wt% and 5 wt%) and SDS (50 ppm and 100 ppm) at Pi = 80 bar. (**a**) To measurement for CH_4 hydrate in the presence of MeOH and SDS at different concentrations. (**b**) Measurement of supercooling of CH_4 hydrate in the presence of MeOH and SDS at different concentrations.

Table 2. Information on dissociation temperature T_d (°C) in the presence of MeOH, SDS, and water under 80 bar. $T_d - T_o$ (°C) indicates the difference between dissociation temperature (T_d) and onset nucleation temperature (T_o).

Chemical Type	CH$_4$ Dissociation (°C)	$T_d - T_o$ (°C)
	80 bar (Fresh)	80 bar (Fresh)
MeOH-A	10.6	1.55
MeOH-B	8.2	1.8
SDS-A	10.8	2.4
SDS-B	10.8	2
Water	11.4	1.75

The data from Table 3 are shown in Figure 4. MeOH-B has the lowest T_d, and pure water has the highest T_d, which is consistent with the conclusion from the measurement of the formation temperature (T_o). The values of the temperature difference, TD = T_d–T_o, are shown in Table 3. It can be observed that TD is lower in the presence of chemicals than in the case of pure water. This indicates a shorter operational temperature window available for hydrate formation and dissociation process in the presence of chemicals. The measured TD is higher for SDS than for MeOH, thus longer operational windows are available to form and dissociate CH_4 hydrate (in the presence of SDS), compared to CH_4 formation and dissociation in the presence of MeOH. Increase in concentration also reduced the T_d and TD, indicating that concentration minimization is beneficial for hydrate formation and dissociation-based processes.

3.1.3. Isothermal for CH_4 Hydrate

The induction time (t_o) is the time length between gas injection and before the start of rapid pressure drop [37]. Information of induction time helps the selection of an optimum additive. Induction time values for fresh and memory runs for CH_4 hydrate formation are summarized in Table 3. Induction time values of repeated experiment runs are generally lower due to the memory effect of water. Thus, faster hydrate film formation at the gas–liquid interface caused the earlier formation of the diffusion barrier at the gas–liquid interface. Therefore, the pressure drop is expected to be lower for the memory run compared to the fresh run. During memory runs, an aqueous solution which has previously

undergone a formation and dissociation sequence is re-used. Isothermal experiments (fresh and memory) are performed at 1 °C (14 h each) and later temperature is dropped to −4 °C to investigate the self-preservation effect.

Table 3. Provides gas uptake (nCH_4 (H)) and total pressure drop (ΔP) in the presence of low dosage MeOH, SDS, and water during fresh and memory runs. Peq = 28.5 bar at 1 °C for CH_4 gas hydrate.

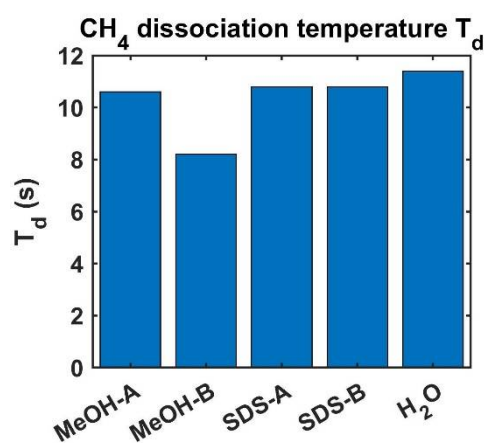|	Gas Uptake at p = 80 bar			
	Fresh		Memory	
	nCH_4 (H)	ΔP (bar)	nCH_4 (H)	ΔP (bar)
MeOH–A	0.032	8.1	0.034	9.3
MeOH–B	0.054	24.7	0.054	24.5
SDS A	0.031	7.7	0.029	5.9
SDS B	0.032	8.0	0.029	6.1
Water	0.032	8.0	0.033	8.6

Figure 4. T_d of different chemicals during SCR using rocking cell setup.

Isothermal experiments were performed for P = 80 and 100 bar, respectively, for two different chemicals (SDS and MeOH). At the lower driving force (P = 80 bar), a promotion effect was observed for MeOH (5 wt%). Similar pressure response curves were observed for fresh and memory run at a lower driving force (P = 80 bar). Under P = 80 bar, MeOH-B shows rapid pressure drops (in fresh and memory run) with its induction time being approximately 8 h, whereas no rapid pressure drop is observed for SDS 100 ppm, MeOH-A, and water. A maximum gas uptake of 54 mmol of CH_4 in hydrate is recorded in the presence of 5 wt% MeOH, compared with 29–33 mmol stored for another system at 80 bar and 1 °C.

At the higher driving force, P = 100 bar, no rapid hydrate pressure drop was observed for the methanol system, which could be due to rapid hydrate film formation (lower induction time) at the gas–liquid interface (see Figure 5). At P = 100 bar, SDS-B and MeOH-A show a rapid pressure drop only for fresh runs, but not for memory runs (see Figure 5). SDS-B (100 ppm) shows a rapid pressure drop only for memory runs when the temperature drops below 0 °C, which is due to additional supercooling. The differences between the hydrate formation behavior for fresh and memory runs show that the induction time is affected by the additives and their concentrations. The induction time increases for SDS-B for a given experimental run time, while it decreases for MeOH-B. A similar observation on induction time was made for CH_4 hydrate formation in sediments [1]. The total pressure drop in the presence of SDS-B is 40 bar and of MeOH-A ~20 bar, which directly correlates with their gas uptake capacity. This gas uptake variation is also positively correlated with the total pressure drop, Pi–Pf (see Figure 5). The total gas uptake in the presence of low concentration MeOH was studied for propane gas, and it was found that the propane gas

uptake rate (µmol/s)j in the hydrate improved when the MeOH concentration in the frozen MeOH-water system increased from 0.016 wt% to 1 wt% [47].
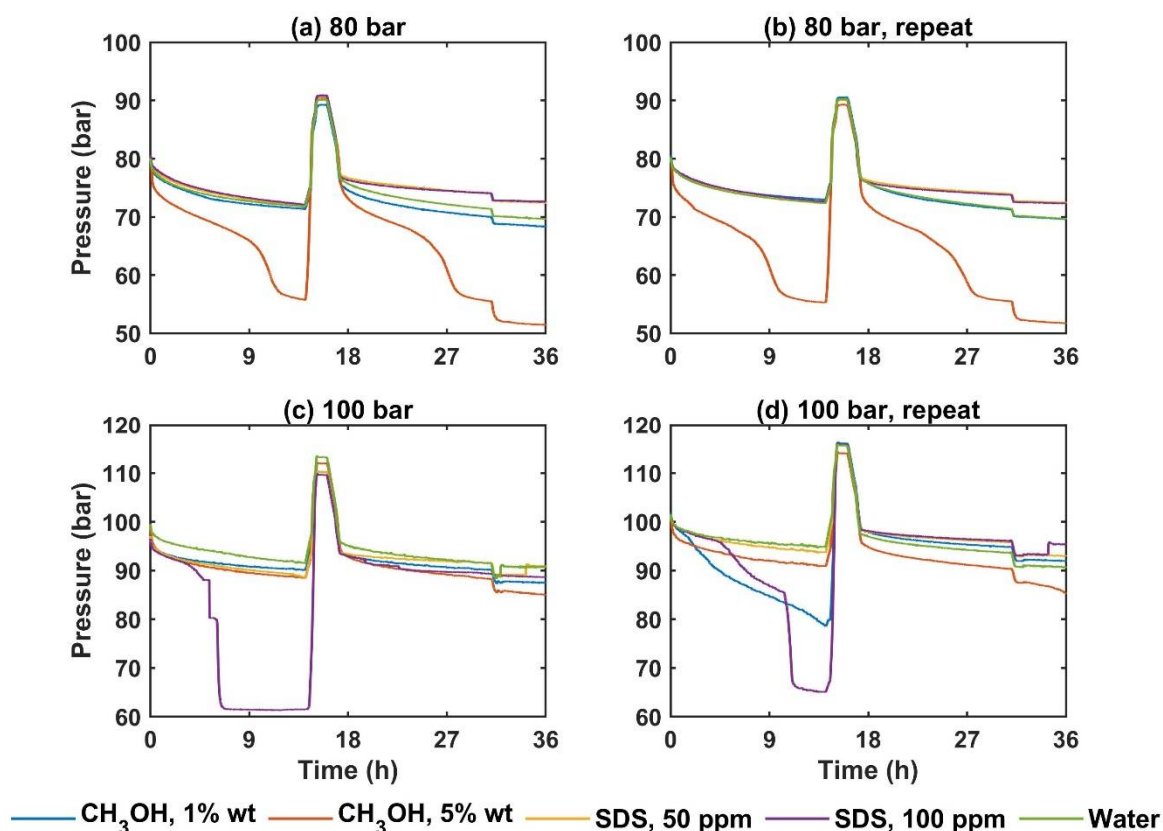

Figure 5. Pressure variation (fresh and memory run) during the isothermal scheme in the presence of MeOH (1 wt%, 5 wt%), SDS (50 ppm, 100 ppm), and pure water. p = 80 bar and 100 bar, T = 1 °C. (**a**,**b**) Pressure profile (fresh and memory) under 80 bar (2 trials) (**c**,**d**) Pressure profile (fresh and memory) under 100 bar (2 trials). Pressure increase above initial pressure is on account of temperature increased from 1 °C to 25 °C. (Starting pressure is pressure at 1 °C).

The thermodynamic inhibition of MeOH is mostly studied in V-L-H (vapor–liquid-hydrate) systems. Little is known about the effect of MeOH on the kinetics of hydrate formation in V-L-H and V-L-I-H (vapor–liquid–ice-hydrate) systems, and the mechanisms of inhibition and promotion have not been thoroughly investigated. To investigate the effect of V-L-I-H systems on kinetics, the temperature was lowered from 1 °C to −4 °C and then remains at −4 °C during the isothermal experiment at Pi = 100 bar (see Figure 6).

Pressure variation (refer to Figure 6) shows a rapid pressure drop for MeOH-B (5 wt%) and no significant pressure drop for other aqueous solutions. As the temperature starts to decrease from 1 °C to −4 °C after 36 h, extra sub-cooling provides an additional driving force for the MeOH-B solution that accelerates the rapid hydrate formation. The total pressure drop at T = −4 °C for MeOH-B (5 wt%) is approximately 25 bar, the second to SDS B (100 ppm) aqueous solution. This additional driving force in the case of MeOH-B was due to no ice formation (caused by the freezing point depression of MeOH-B) during the cooling to −4 °C. In general, 5 wt% MeOH and 1 wt% MeOH have freezing point depressions equal to −3.0 °C and −0.5 °C, respectively. No freezing point depression is observed for SDS.
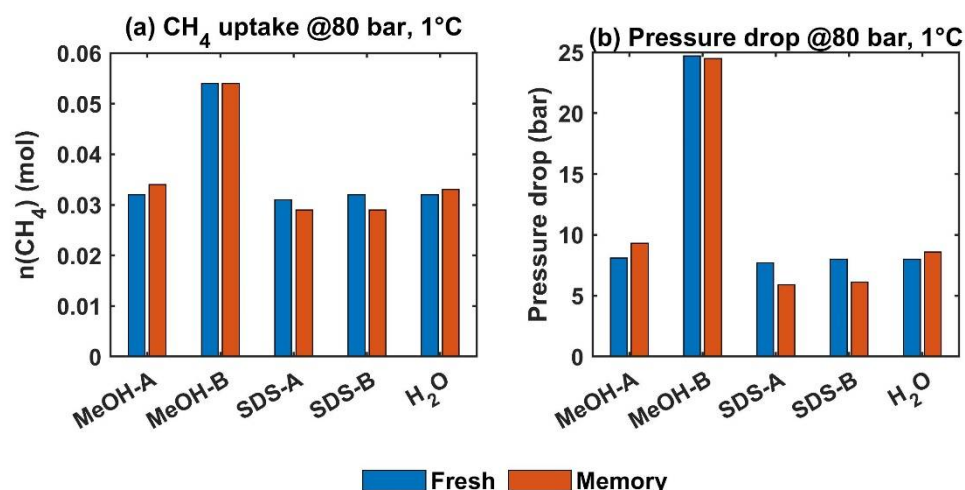
Figure 6. Total gas uptake during the isothermal temperature scheme in the presence of MeOH (A and B). The experimental temperature at 1 °C, (**a**) Total CH_4 gas uptake during isothermal under 80 bar, (**b**) Total pressure drop during Isothermal under P = 80 bar.

Table 4 provides a total pressure drop during the SCR (T = 25 °C–1 °C) and isothermal (T = 1 °C) run under 80 bar. Uncertainty in pressure response during isothermal experiments suggests that isothermal experiments have poor reproducibility compared with the SCR technique due to the weaker promotion ability of the chemicals (at the low concentration).

Table 4. Total pressure drop in the presence of MeOH, SDS, and water during fresh runs at T = 1 °C and for P = 80 bars.

	IT	SCR
	ΔP (bar)	ΔP (bar)
MeOH–A	8.1	12
MeOH–B	24.7	20
SDS A	7.7	12
SDS B	8.0	44
Water	8.0	11

Comparing results for P = 80 bar, the highest gas uptake (highest pressure drop during fresh run) was measured for SDS-B (100 ppm), followed by MeOH B (5 wt%). An increase in initial operating pressure would provide an additional driving force that could accelerate the gas uptake in hydrates. It should be noted that due to the memory effect, a lower induction time indicates accelerated hydrate film formation at the gas–liquid interface. Therefore, a repeated run with a stronger memory effect is expected to have a shorter pressure drop than a new run due to the (accelerated) formation of a diffusion barrier.

3.1.4. CH_4 Dissociation Behavior at T < 0 °C

The rocking cell system is a closed system volume, and dissociation experiments are performed on a constant volume system so that dissociation behavior might be observed via increasing the rate of system pressure. Such a technique to observe dissociation has been tested by various groups previously [45,48]. The dissociation behavior of gas hydrates below 0 °C is of great value for understanding hydrate stability under self-preservation tendency with and without additives. The dissociation of hydrates at T < 0 °C is slower than at T > 0 °C due to self-preservation, hydrate metastability, and secondary hydrate/ice formation [49]. CH_4 hydrate formation studies have been investigated in the presence of different additives; however, dissociation behavior and CH_4 hydrate self-preservation tendency have been investigated only by few. For example, CH_4 hydrates dissociation studies in the presence of an electrolyte (NaCl, $MgCl_2$, Na_2SO_4) [50–52] show that a higher

electrolyte concentration weakens self-preservation. The effect of SDS on CO_2 hydrate self-preservation [53] and CH_4 hydrate self-preservation [54] has also been studied. Self-preservation is also dependent on the type of guest molecules [55,56]. The effect of MeOH and SDS (at low dosage) on hydrate dissociation at T < 0 °C has not yet been tested and discussed in detail.

To investigate the effect of additives on hydrate dissociation at T < 0 °C, we performed dissociation experiments at T = −2 °C and T = −4 °C. Dissociation experiments below 0 °C are an extended version of the isothermal experiments at 1 °C. After calculating the gas uptake at 1 °C, the temperature is lowered below 0 °C and the systems are left idle for a few hours until the pressure stabilizes. Following this, the pressure is quickly reduced to atmospheric pressure and the pressure rebound curve is recorded. Figure 7 shows the pressure curve for Pi= 80 bar at T = −2 °C and Pi= 100 bar at T = −4 °C. At T = −2 °C, the vapor–ice-hydrate system (V-I-H) is present in all samples except MeOH-B (V-L-H). At T = −4 °C, the vapor–ice-hydrate system (V-I-H) is present in all samples.
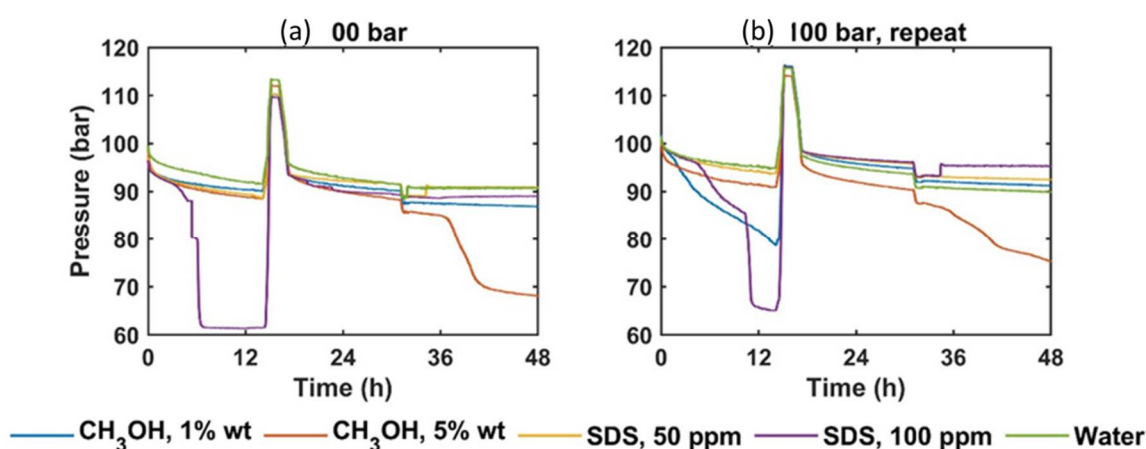

Figure 7. Pressure variation during temperature reduction from 1 °C to −4 °C during the isothermal experiment. Temperature reduces to −4 °C after 30 h. (**a**,**b**) show the pressure variation during the first and second trial. The pressure increase above initial pressure is on account of temperature increased from 1 °C to 25 °C. (Starting pressure is pressure at 1 °C).

Previous studies show that dissociation behavior below the freezing point is affected by guest molecules, hydrate saturation, pressure and temperature conditions, and the presence of chemicals [57–60]. The increase in pressure profile shows the increase in pressure during the dissociation of CH_4 hydrate. Figure 8 shows that the pressure increases rapidly (fast dissociation) and reaches a stable line with time. This could be due to reaching the equilibrium state or ice formation on the surface of the hydrates. In Figure 7a, comparison of different pressure curves at T = −2 °C shows different dissociation behavior. CH_4 hydrate in the presence of MeOH B has no ice in the system (V-L-H, no ice due to freezing point depression) and therefore dissociates faster than SDS/water/MeOH A (the pressure curve between MeOH B and others is wide). High-hydrate saturation also contributed to faster dissociation (high-gas uptake during cooling below 0 °C). In the case of the presence of hydrate and water (absence of ice), water saturation also influences hydrate dissociation behavior [61].
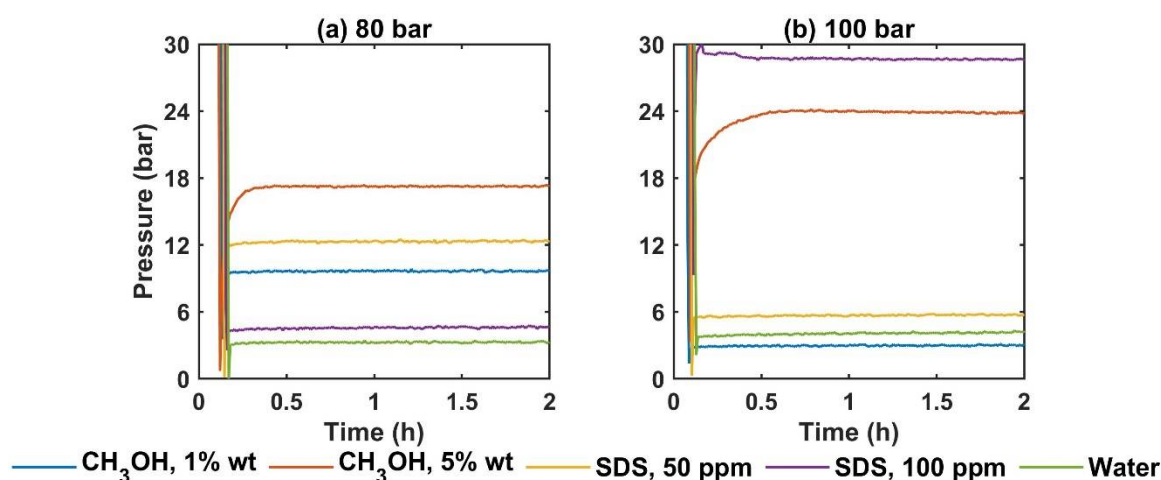
Figure 8. Pressure behavior of CH_4 hydrate at T = $-2\,°C$ and T = $-4\,°C$ after the system of hydrate and ice is rapidly expanded to atmospheric pressure. Self-preservation is studied at T = $-2\,°C$ and T = $-4\,°C$. (**a**) Pressure response curve for Pi = 80 bar, T = $-2\,°C$ (**b**) Pressure response curve for Pi = 100 bar, T = $-4\,°C$.

The pressure response curve at T = $-4\,°C$ (only V-I-H system present) and the hydrate based on SDS dissociated the fastest compared to MeOH and water. Between SDS A and SDS B, SDS B dissociated faster than SDS A. Although SDS B (100 ppm) and MeOH B have a comparable gas uptake, the different dissociation behavior at T = $-4\,°C$ clearly shows the weaker self-preservation due to the presence of SDS. The weaker self-preservation effect due to the presence of SDS has been confirmed in other similar studies for CO_2 hydrates and CH_4 hydrates [45,53]. As our system is identified as a low-hydrate saturation based system, our conclusion is based on the assumption that for the low-hydrate saturation case, the effect of a different hydrate saturation, hydrate morphology, and hydrate surface area is at a minimum across all samples [62]. Therefore, we believe that more detailed studies are needed to investigate the effect of hydrate saturation and morphology (due to the presence of chemicals) on self-preservation. Compared to the additive-based solutions, the pure water solution showed the lowest pressure decrease and increase and the slowest dissociation profile curve due to the low-hydrate saturation and high-ice saturation. Detailed discussion about self-preservation and the effect of different factors are also available in our previous two manuscripts on similar topics [45,49].

3.2. CO_2/N_2 Formation and Dissociation Kinetics

CO_2/N_2 formation and dissociation kinetics may be important for both CO_2/N_2 injection into CH_4 hydrate and CO_2 capture from the CO_2/N_2 gas stream. Although there are several studies on the formation kinetics of CO_2/N_2 hydrate using different additives (silica gel, amino acids, surfactants) [21,63], the effect of low-dosage MeOH on CO_2 capture from CO_2/N_2 using gas hydrate technology is still unexplored. Therefore, in this section, CO_2/N_2 hydrate formation and dissociation kinetics are investigated in the presence of MeOH.

3.2.1. Onset Temperature (T_o) and Subcooling ΔT_{sub} for CO_2/N_2 Hydrate

The onset temperature for CO_2/N_2 hydrate was studied under P = 120 bar and 100 bar, respectively, and summarized in Table 5. T_o was calculated for different concentrations of MeOH and SDS under P_i = 120 bar and 100 bar, respectively. Pressure variation (for Pi = 120 bar and two trials) during SCR is presented in Figure 9.

Table 5. Onset nucleation temperature To (°C) (averaged) and sub (ΔT_{sub}) for CO_2/N_2 hydrate in the presence of MeOH and SDS (T_{eq} = 6.32 °C for 120 bar and T_{eq} = 5.11 °C for 100 bar); NF = No formation.

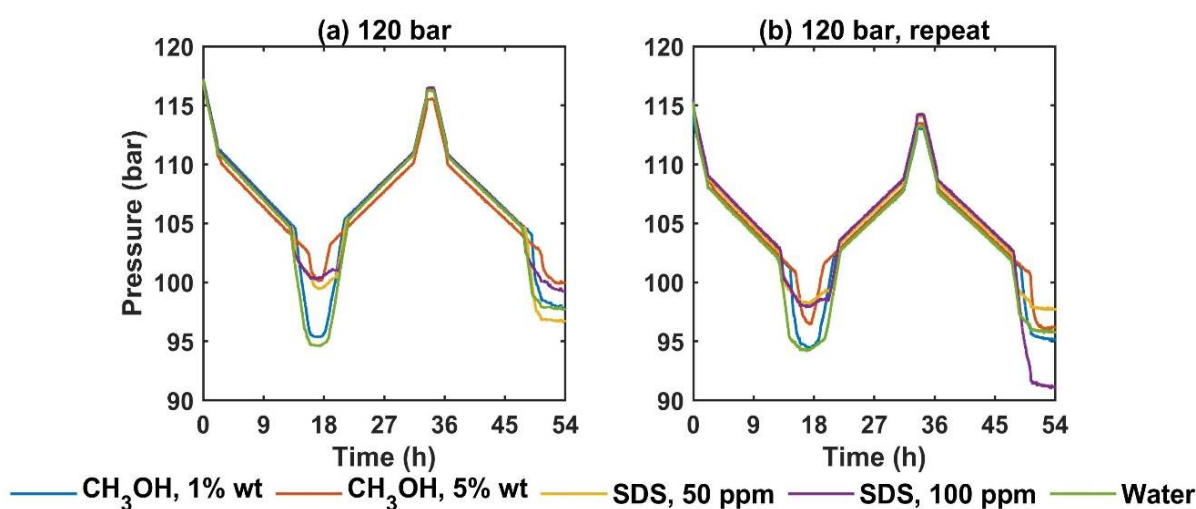|	CO_2/N_2 Formation Kinetics (Using 20 mol% CO_2 in CO_2/N_2 Mixture)							
	100 bar				120 bar			
	Fresh		Memory		Fresh		Memory	
	T_o (°C)	ΔT_{sub} (°C)	T_o (°C)	ΔT_{sub} (°C)	T_o (°C)	ΔT_{sub} (°C)	T_o (°C)	ΔT_{sub} (°C)
MeOH-A	2.5	2.6	2.2	3.6	2.8	3.6	2.7	3.7
MeOH-B	NF	NF	NF	NF	1.3	5.1	1.0	5.3
SDS-A	2	3.1	1.8	3.4	3.7	2.7	3.6	2.8
SDS-B	2	3.1	1.9	3.3	3.6	2.7	3.6	2.7
Water	3.3	1.8	3.1	4.3	4.2	2.2	4.1	2.3

Figure 9. Pressure profiles during the constant ramping temperature scheme in the presence of MeOH, SDS, and water at 120 bar. Starting temperature 25 °C and final temperature 1 °C. Temperature ramping rate 1 °C/h between 15 °C–1 °C. (**a**,**b**) starting pressure 120 bar, fresh, and repeat the experiment.

SCR was conducted under Pi = 100 bar and Pi = 120 bar to facilitate CO_2/N_2 hydrate formation. In the case of a low driving force (lower starting pressure, Pi = 100 bars), presence of MeOH-B (5 wt%) did not cause any promotion effect (No non-linear pressure drop, NF). This can be attributed to the MeOH-B inhibition effect at a higher concentration being more visible at a low-driving force. When the driving force increased to Pi = 120 bars, a non-linear pressure drop was observed for each chemical and water. The key advantage of SCR method is to slowly form the hydrate film at the gas–liquid interface and thus maximize the gas diffusion by delaying the diffusion barrier.

Figure 6 shows that pressure drops are the highest for MeOH-A (1 wt%) and water. Other additives, including SDS A, SDS B, and MeOH B have similar pressure drops. The low pressure drop in the presence of SDS could be due to an earlier onset of nucleation, which creates a thicker barrier for mass transfer compared to MeOH and water. The pressure variations during the SCR experiment suggest that the delayed nucleation does not contribute to the lower gas uptake due to the different morphology of the hydrate film at the gas–liquid interface. Therefore, water and MeOH were more suitable than SDS for promoting CO_2/N_2 hydrates.

Table 5 is illustrated in Figure 10. At Pi = 120 bar, the lowest T_o is observed for MeOH-B, while the highest To is observed for water. This indicates that the presence of chemicals delays the nucleation, as compared to water. Delay in nucleation on account of the chemicals has been observed in our previous publications too [21,45,64]. In general,

CO_2/N_2 hydrate in the presence of amino acids (hydrophobic and hydrophilic) had a higher onset nucleation temperature (To~3.9 to 5.4 °C for amino acids) and for SDS (To~3.8 to 5.8 °C) during the formation [21].

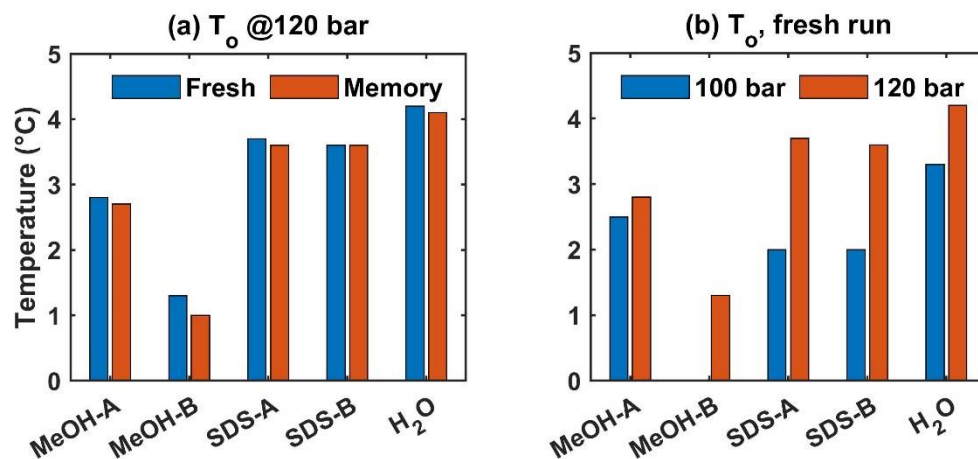**Figure 10.** T_o under 120 and 100 bar for fresh and memory runs. (**a**) Onset temperature T_o under 120 bar for fresh and memory runs. (**b**) T_o during fresh runs under 100 bar and 120 bar, respectively.

In general, MeOH had a strong inhibition effect compared to SDS, indicated by the delayed onset nucleation temperature compared to SDS. A further increase in MeOH concentration (from 1 wt% to 5 wt%)—and T_o decreased from 2.8 to 1.3 °C at 120 bar—suggests a stronger inhibition effect at the higher concentration. This indicates the inhibition nature of MeOH. When the SDS concentration increases from 50 ppm to 100 ppm, no significant change in T_o is observed. When pressure increases from 100 bar to 120 bar, T_o increases for all chemicals; we can say that for CO_2/N_2 gas hydrate, T_o depends on MeOH concentration and pressure. The lower the MeOH concentration, the higher in the T_o.

3.2.2. The Onset of Dissociation Temperature (T_d)

Table 6 lists the average T_d for MeOH, SDS, and water under 120 and 100 bar. T_d under different pressure for MeOH, SDS, and water is presented in Figure 8.

Table 6. Dissociation temperature T_d (°C) in the presence of MeOH and SDS for two different concentrations.

Chemical Type	CO_2/N_2 Dissociation Temp		Deviation $T_d - T_o$	
	120 bar	**100 bar**	**120 bar**	**100 bar**
MeOH-A	4.6	3.6	1.8	1.1
MeOH-B	2.5	n.a	1.2	n.a
SDS-A	5.1	3.4	1.5	1.4
SDS-B	5.0	3.3	1.4	1.3
Water	5.4	4.3	1.3	1

The T_d values at different concentrations of additives and different pressures are shown in Figure 11. In general, a low T_d value indicates low hydrate stability; with increasing temperature, hydrates with lower Td values dissociate first. Below 100 bar, no hydrate formation is observed for MeOH-B; thus, there is no dissociation temperature. Figure 11 shows that the highest T_d for pure water is observed at pressures of 120 and 100 bar. Below 120 bar, the lowest T_d is observed for MeOH. At 100 bar, the lowest T_d is observed for SDS -B. The T_d–T_o values are listed in Table 6. As the pressure increases, T_d–T_o increases. In the case of CO_2/N_2, the highest T_d–T_o is observed for MeOH below 120 bar, while the lowest T_d–T_o is found for MeOH B.
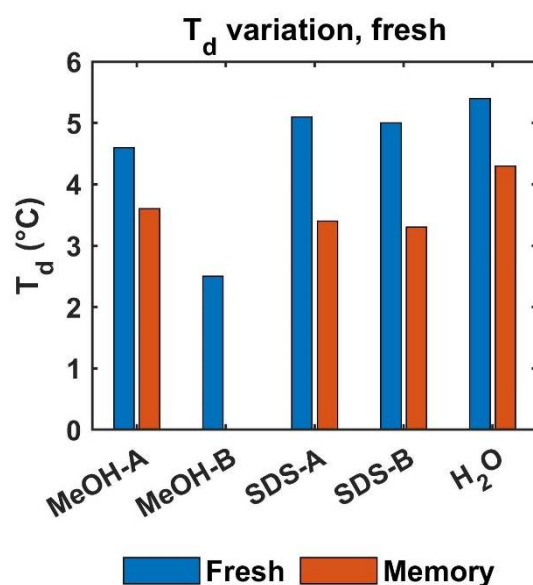
Figure 11. Illustrated T_d measurement for different chemicals during SCR using rocking cell setup.

3.2.3. Isothermal for CO_2/N_2 Hydrate

The hydrate-formation condition for the CO_2 rich mixture (CO_2-N_2) with 20 mol% CO_2 in the presence of aqueous solutions of MeOH (1 wt% & 5 wt%) was investigated within the pressure range of 120 bar–100 bar and T = 1 °C. Overall pressure response during the isothermal experiments is presented in Figure 12. Two trials were performed at 100 bar and 120 bar. The reported value is averaged and presented in Table 7. The experiments at 80 bar do not show hydrate formation for any additive or pure water during the given experimental time; therefore, they are excluded from the discussion.
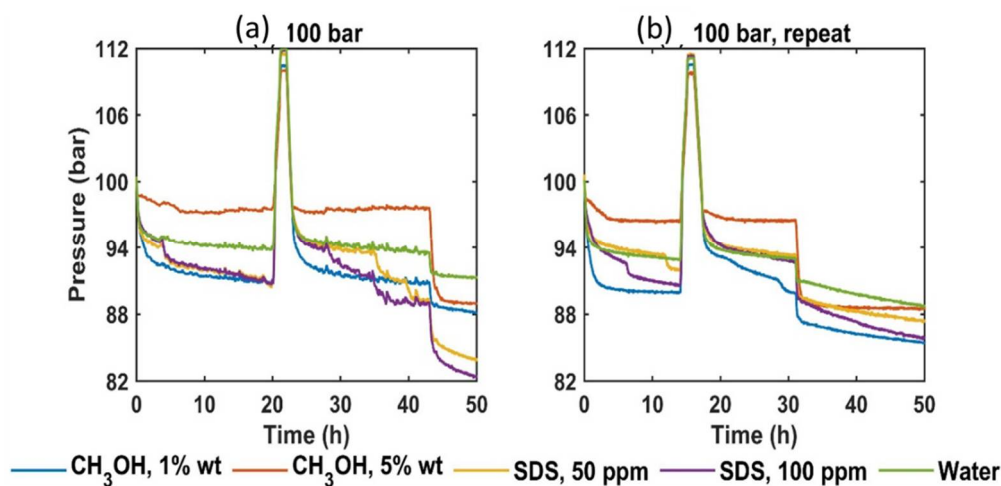

Figure 12. Pressure variation for CO_2/N_2 gas mixture using 20 mol% CO_2 during the isothermal scheme in the presence of MeOH (1, 5 wt.%) and SDS (1, 5 wt%) at 80 bar. Each temperature cycle runs for more than 14 h. Heating and cooling are done without replacing the sample to study the effect on the used sample. GC samples are collected by cooling down the system at T = −2 °C. The pressure response curves for 100 bar are shown in the figure (**a,b**). Similar curves are recorded for 120 bar as well. No rapid pressure drop is observed for *p* = 80 bar when water or additives are present. Pressure increase above initial pressure is on account of temperature increased from 1 °C to 25 °C. (Starting pressure are the pressure at 1 °C).

Table 7. Provide CO_2 gas uptake in hydrate calculations in the presence of MeOH (1 wt%, 5 w%) and SDS (50 ppm, 100 ppm) and pure water. $\Delta P1$ is total pressure drops at T = −2 °C, $\Delta P2$ is total pressure drop at T = 1 °C. Induction time measured at T = 1 °C, ΔCO_2 (H) = CO_2 moles in hydrate, $\Delta CO_2\%$ = capture efficiency.

	Gas Uptake Calculations			
	$\Delta P1$ (bar)	$\Delta P2$ (bar)	ΔCO_2 (H) (mol) $\times 10^{-3}$	$\Delta CO_2\%$
P_i = 120 bar				
MeOH-A	15.5	9.6	19.1	54%
MeOH-B	15.4	7.4	22.2	63%
SDS-A	12.9	9.3	32.4	92%
SDS-B	35.1	14.7	33.0	93%
Water	12.5	9.1	16.9	48%
P_i = 100 bar				
MeOH-A	14.0	6.0	19.2	66%
MeOH-B	11.4	2.8	17.1	59%
SDS-A	15.3	4.0	20.4	70%
SDS-B	18.1	4.6	21.5	73%
Water	10.6	4.3	15.3	52%

Table 7 provides the key measurement data, including total gas uptake, total CO_2 mole capture, and CO_2 capture efficiency at P =120 and 100 bar using GC analysis (at T = −2 °C) during isothermal experiments.

The pressure drops are measured for T = 1 °C and T = −2 °C, since a temperature drop below 0 °C leads to an unprecedented pressure profile (as shown in Figure 12). At T = −2 °C, no ice formation is expected due to the freezing point depression of water in the presence of MeOH-A, while ice is expected in the presence of water and SDS. The presence or absence of ice at T = −2 °C results in a different pressure response as the temperature drops from 1 °C to −2 °C. At T = −2 °C, gas samples are taken quickly during sampling to avoid gas contamination. GC analysis is used to calculate the CO_2 gas molecule in the hydrate in the presence of water and various additives.

The table above suggests that total gas uptake in case of SDS system is higher than MeOH. Higher gas uptake value is complemented by higher CO_2 capture efficiency in hydrate in the presence of SDS. For example, for SDS, CO_2 capture efficiency is around 90% while for the MeOH system, capture efficiency is around 60% at 120 bar. Reduction in pressure from 120 bar to 100 bar leads to a decrease in total gas uptake for both additives. For SDS, CO_2 capture efficiency falls from 90% to 70%, while CO_2 capture efficiency does not vary for MeOH. For SDS, CO_2 selectivity is higher than N_2 at 120 bar, which decreases with pressure.

4. Application of MeOH for CH_4 Recovery by CO_2 Injection

The available literature suggests that when MeOH is injected into added into CH_4 hydrate reservoir. It is documented through this study and previous studies that when in a concentration below 10 wt%, MeOH shows delayed kinetic promotion effect. Compared with a known promoter such as SDS, its promotion capabilities can be characterized as moderate-to-low for pressure above 80 bar. Additionally, the MeOH promotion capability also depends on guest molecules. MeOH at 5 wt% shows better promotion capability for CH_4 gas hydrate compared with CO_2/N_2. While at 1 wt%, MeOH shows better promotion capability for CO_2/N_2 than CH_4. This difference in promotion capabilities could be useful in CH_4 extraction from the hydrate reservoir by CO_2 injection. A recent experimental study has shown enhanced CH_4 recovery and CO_2 storage in the presence of 5 wt% MeOH when CO_2 is injected into sedimentary CH_4 hydrate [1]. The presence of 5 wt% MeOH in residual pore water is advantageous as it delays CO_2 hydrate film formation at injection wells, thus allowing better CO_2 injectivity into CH_4. CH_4 gas released from either CH_4 hydrate dissociation or from CH_4-CO_2 hydrate swapping is less likely to form a mixed

hydrate in the CH_4-CO_2-H_2O system, and thus recovery is enhanced. (See Figure 13 for a conceptual schematic).
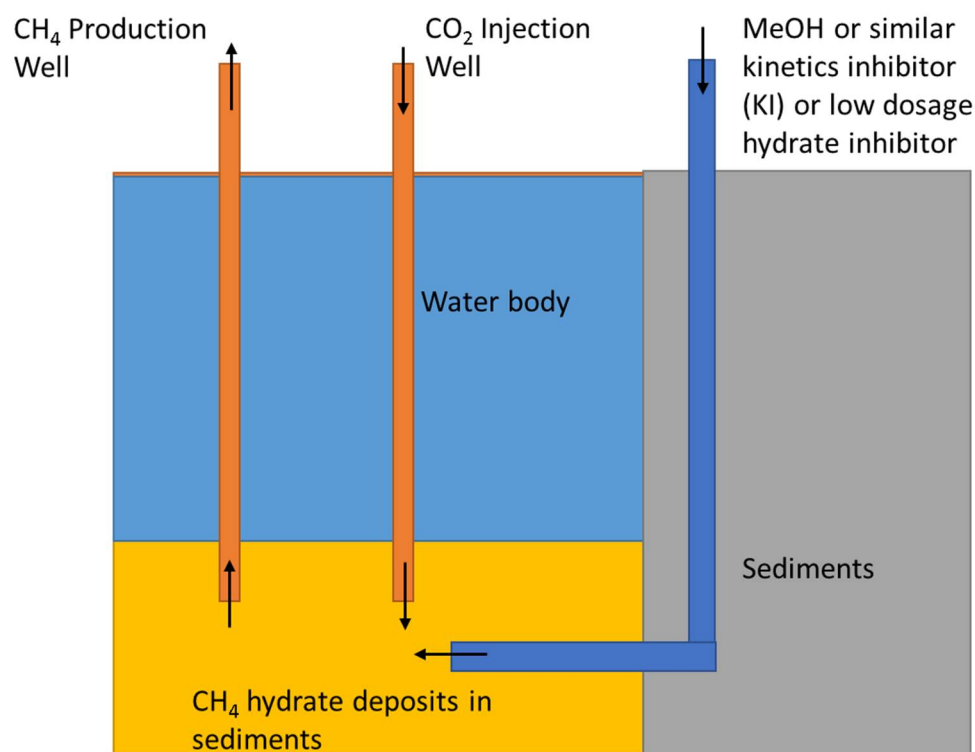

Figure 13. Conceptual schematic of additive-supported CO_2 injection into CH_4 hydrate for enhanced CH_4-CO_2 hydrate swapping.

Gang Li et al. [65] studied the effects of methanol injection on the dissociation behavior of CH_4 hydrates. In this study, no further CO_2 injection was performed, and the overall CH_4 dissociation behavior was divided into 4 stages. There was also a direct correlation between the methanol injection rate and production efficiency. Therefore, further studies need to be conducted where methanol is injected into the CH_4 hydrate, followed by CO_2 injection. According to another study [66], the rate of hydrate dissociation is a function of additive concentration, injection rate, pressure, temperature, and the additive–hydrate interface. Therefore, it is extremely important that detailed laboratory studies be conducted to avoid large-scale hydrate dissociation and possible environmental contamination from additive injection.

5. Conclusions

Studies have confirmed the role of MeOH as a hydrate promoter when used at low concentration. The effects of MeOH concentration (1 wt% to 5 wt%) on kinetic parameters such as onset temperature, induction time, and gas uptake were measured for both CH_4 and CO_2/N_2 gas mixtures. The promotion capability of MeOH was comparable to SDS (50 ppm, 100 ppm). The results showed that the promotion of CH_4 hydrates was stronger in the presence of MeOH at a higher concentration (5 wt%), while the promotion of CO_2-N_2 hydrates was stronger in the presence of MeOH at a lower concentration (1 wt%). Thus, MeOH (at 5 wt%) is a better candidate for injection into the CH_4 hydrate (delayed CH_4 hydrate dissociation and CO_2/N_2 hydrate formation), allowing additional gas injection into the system. This conclusion agrees well with our previous results demonstrating optimal CH_4 recovery and CO_2 storage in the presence of 5 wt% MeOH. The experimental observations of this study help in exploring the use of MeOH and similar alcohols to enhance CH_4-CO_2 hydrate exchange.

References

1. Pandey, J.S.; Karantonidis, C.; Karcz, A.P.; von Solms, N. Enhanced CH_4-CO_2 Hydrate Swapping in the Presence of Low Dosage Methanol. *Energies* **2020**, *13*, 5238. [CrossRef]
2. Khlebnikov, V.N.; Antonov, S.V.; Mishin, A.S.; Bakulin, D.A.; Khamidullina, I.V.; Liang, M.; Vinokurov, V.A.; Gushchin, P.A. A new method for the replacement of CH4 with CO_2 in natural gas hydrate production. *Nat. Gas Ind. B* **2016**, *3*, 445–451. [CrossRef]
3. Gauteplass, J.; Almenningen, S.; Barth, T.; Ersland, G. Hydrate Plugging and Flow Remediation during CO_2 Injection in Sediments. *Energies* **2020**, *13*, 4511. [CrossRef]
4. Pandey, J.S.; Daas, Y.J.; Karcz, A.P.; von Solms, N. Enhanced Hydrate-Based Geological CO_2 Capture and Sequestration as a Mitigation Strategy to Address Climate Change. *Energies* **2020**, *13*, 5661. [CrossRef]
5. Pandey, J.S.; Ouyang, Q.; Solms, N. von New insights into the dissociation of mixed CH4/CO2 hydrates for CH_4 production and CO2 storage. *Chem. Eng. J.* **2022**, *427*, 131915. [CrossRef]
6. Vasheghani Farahani, M.; Hassanpouryouzband, A.; Yang, J.; Tohidi, B. Insights into the climate-driven evolution of gas hydrate-bearing permafrost sediments: Implications for prediction of environmental impacts and security of energy in cold regions. *RSC Adv.* **2021**, *11*, 14334–14346. [CrossRef]
7. Bobev, S.; Tait, K.T. Methanol—inhibitor or promoter of the formation of gas hydrates from deuterated ice? *Am. Mineral.* **2004**, *89*, 1208–1214. [CrossRef]
8. McLaurin, G.; Shin, K.; Alavi, S.; Ripmeester, J.A. Antifreezes Act as Catalysts for Methane Hydrate Formation from Ice. *Angew. Chem.* **2014**, *126*, 10597–10601. [CrossRef]
9. Devlin, J.P. Catalytic activity of methanol in all-vapor subsecond clathrate-hydrate formation. *J. Chem. Phys.* **2014**, *140*, 164505. [CrossRef]
10. Kvamme, B.; Selvåg, J.; Saeidi, N.; Kuznetsova, T. Methanol as a hydrate inhibitor and hydrate activator. *Phys. Chem. Chem. Phys.* **2018**, *20*, 21968–21987. [CrossRef]
11. Buch, V.; Devlin, J.P.; Monreal, I.A.; Jagoda-Cwiklik, B.; Uras-Aytemiz, N.; Cwiklik, L. Clathrate hydrates with hydrogen-bonding guests. *Phys. Chem. Chem. Phys.* **2009**, *11*, 10245. [CrossRef]
12. Williams, K.D.; Devlin, J.P. Formation and spectra of clathrate hydrates of methanol and methanol-ether mixtures. *J. Mol. Struct.* **1997**, *416*, 277–286. [CrossRef]
13. Blake, D.; Allamandola, L.; Sandford, S.; Hudgins, D.; Freund, F. Clathrate Hydrate Formation in Amorphous Cometary Ice Analogs in Vacuo. *Science* **1991**, *254*, 548–551. [CrossRef]
14. Veluswamy, H.P.; Kumar, A.; Seo, Y.; Lee, J.D.; Linga, P. A review of solidified natural gas (SNG) technology for gas storage via clathrate hydrates. *Appl. Energy* **2018**, *216*, 262–285. [CrossRef]
15. Sadeq, D.; Iglauer, S.; Lebedev, M.; Smith, C.; Barifcani, A. Experimental determination of hydrate phase equilibrium for different gas mixtures containing methane, carbon dioxide and nitrogen with motor current measurements. *J. Nat. Gas Sci. Eng.* **2017**, *38*, 59–73. [CrossRef]
16. Pan, Z.; Liu, Z.; Zhang, Z.; Shang, L.; Ma, S. Effect of silica sand size and saturation on methane hydrate formation in the presence of SDS. *J. Nat. Gas Sci. Eng.* **2018**, *56*, 266–280. [CrossRef]
17. Chong, Z.R.; Yang, S.H.B.; Babu, P.; Linga, P.; Li, X. Sen Review of natural gas hydrates as an energy resource: Prospects and challenges. *Appl. Energy* **2016**, *162*, 1633–1652. [CrossRef]
18. Pandey, J.; Solms, N. Hydrate Stability and Methane Recovery from Gas Hydrate through CH_4–CO_2 Replacement in Different Mass Transfer Scenarios. *Energies* **2019**, *12*, 2309. [CrossRef]
19. Jensen, L.; Thomsen, K.; Von Solms, N. Inhibition of structure I and II gas hydrates using synthetic and biological kinetic inhibitors. *Energy Fuels* **2011**, *25*, 17–23. [CrossRef]
20. Brown, T.D.; Taylor, C.E.; Bernardo, M.P. Rapid Gas Hydrate Formation Processes: Will They Work? *Energies* **2010**, *3*, 1154–1175. [CrossRef]
21. Pandey, J.S.; Daas, Y.J.; von Solms, N. Screening of amino acids and surfactant as hydrate promoter for CO_2 capture from flue gas. *Processes* **2020**, *8*, 124. [CrossRef]
22. Pandey, J.S.; Daas, Y.J.; Solms, N.V. Insights into Kinetics of Methane Hydrate Formation in the Presence of Surfactants. *Processes* **2019**, *7*, 598. [CrossRef]

23. Okutani, K.; Kuwabara, Y.; Mori, Y.H. Surfactant effects on hydrate formation in an unstirred gas/liquid system: An experimental study using methane and sodium alkyl sulfates. *Chem. Eng. Sci.* **2008**, *63*, 183–194. [CrossRef]
24. Zhong, Y.; Rogers, R.E. Surfactant effects on gas hydrate formation. *Chem. Eng. Sci.* **2000**, *55*, 4175–4187. [CrossRef]
25. Sadeq, D.; Alef, K.; Iglauer, S.; Lebedev, M.; Barifcani, A. Compressional wave velocity of hydrate-bearing bentheimer sediments with varying pore fillings. *Int. J. Hydrog. Energy* **2018**, *43*, 23193–23200. [CrossRef]
26. Schramm, L.L.; Stasiuk, E.N.; Marangoni, D.G. Surfactants and their applications. *Annu. Rep. Prog. Chem. Sect. C* **2003**, *99*, 3–48. [CrossRef]
27. Zhang, J.S.; Lee, S.; Lee, J.W. Solubility of sodium dodecyl sulfate near propane and carbon dioxide hydrate-forming conditions. *J. Chem. Eng. Data* **2007**, *52*, 2480–2483. [CrossRef]
28. Demissie, H.; Duraisamy, R. Effects of electrolytes on the surface and micellar characteristics of Sodium dodecyl sulphate surfactant solution. *J. Sci. Innov. Res.* **2016**, *5*, 208–214. [CrossRef]
29. Hassanpouryouzband, A.; Joonaki, E.; Vasheghani Farahani, M.; Takeya, S.; Ruppel, C.; Yang, J.; English, N.J.; Schicks, J.M.; Edlmann, K.; Mehrabian, H.; et al. Gas hydrates in sustainable chemistry. *Chem. Soc. Rev.* **2020**, *49*, 5225–5309. [CrossRef]
30. Linga, P.; Clarke, M.A. A Review of Reactor Designs and Materials Employed for Increasing the Rate of Gas Hydrate Formation. *Energy Fuels* **2017**, *31*, 1–13. [CrossRef]
31. Sa, J.H.; Melchuna, A.; Zhang, X.; Morales, R.; Cameirao, A.; Herri, J.M.; Sum, A.K. Rock-Flow Cell: An Innovative Benchtop Testing Tool for Flow Assurance Studies. *Ind. Eng. Chem. Res.* **2019**, *58*, 8544–8552. [CrossRef]
32. Qureshi, M.F.; Khraisheh, M.; Almomani, F. Doping amino acids with classical gas hydrate inhibitors to facilitate the hydrate inhibition effect at low dosages. *Greenh. Gases Sci. Technol.* **2020**, *10*, 783–794. [CrossRef]
33. Bell, S. *Good Practice Guide No. 11—Introductory Guide to Uncertainty of Measurement*; NPL: Teddington, UK, 2001.
34. Daraboina, N.; Pachitsas, S.; Von Solms, N. Experimental validation of kinetic inhibitor strength on natural gas hydrate nucleation. *Fuel* **2015**, *139*, 554–560. [CrossRef]
35. Daraboina, N.; Von Solms, N. The combined effect of thermodynamic promoters tetrahydrofuran and cyclopentane on the kinetics of flue gas hydrate formation. *J. Chem. Eng. Data* **2015**, *60*, 247–251. [CrossRef]
36. Qureshi, M.F.; Atilhan, M.; Altamash, T.; Tariq, M.; Khraisheh, M.; Aparicio, S.; Tohidi, B. Gas Hydrate Prevention and Flow Assurance by Using Mixtures of Ionic Liquids and Synergent Compounds: Combined Kinetics and Thermodynamic Approach. *Energy Fuels* **2016**, *30*, 3541–3548. [CrossRef]
37. Lone, A.; Kelland, M.A. Exploring kinetic hydrate inhibitor test methods and conditions using a multicell steel rocker rig. *Energy Fuels* **2013**, *27*, 2536–2547. [CrossRef]
38. Servio, P.; Englezos, P. Effect of temperature and pressure on the solubility of carbon dioxide in water in the presence of gas hydrate. *Fluid Phase Equilib.* **2001**, *190*, 127–134. [CrossRef]
39. Hashemi, S.; Macchi, A.; Bergeron, S.; Servio, P. Prediction of methane and carbon dioxide solubility in water in the presence of hydrate. *Fluid Phase Equilib.* **2006**, *246*, 131–136. [CrossRef]
40. Servio, P.; Englezos, P. Measurement of Dissolved Methane in Water in Equilibrium with Its Hydrate. *J. Chem. Eng. Data* **2002**, *47*, 87–90. [CrossRef]
41. Kelland, M.A. History of the development of low dosage hydrate inhibitors. *Energy Fuels* **2006**, *20*, 825–847. [CrossRef]
42. Ballard, A.L.; Sloan, E.D. The Next Generation of Hydrate Prediction: An Overview. *J. Supramol. Chem.* **2002**, *2*, 385–392. [CrossRef]
43. Pandey, J.S.; Daas, Y.J.; Von Solms, N. Methane hydrate formation, storage and dissociation behavior in unconsolidated sediments in the presence of environment-friendly promoters. In Proceedings of the Society of Petroleum Engineers—SPE Europec Featured at 82nd EAGE Conference and Exhibition, Online, 18–21 October 2021.
44. Sloan, E.D., Jr.; Koh, C.A.; Koh, C.A. *Clathrate Hydrates of Natural Gases*, 3rd ed.; CRC Press: Boca Raton, FL, USA, 2007; ISBN 9780429129148.
45. Pandey, J.S.; Khan, S.; Solms, N. Von Chemically Influenced Self-Preservation Kinetics of CH4 Hydrates below the Sub-Zero Temperature. *Energies* **2021**, *14*, 6765. [CrossRef]
46. Sloan, E.D.; Subramanian, S.; Matthews, P.N.; Lederhos, J.P.; Khokhar, A.A. Quantifying hydrate formation and kinetic inhibition. *Ind. Eng. Chem. Res.* **1998**, *37*, 3124–3132. [CrossRef]
47. Amtawong, J.; Guo, J.; Hale, J.S.; Sengupta, S.; Fleischer, E.B.; Martin, R.W.; Janda, K.C. Propane Clathrate Hydrate Formation Accelerated by Methanol. *J. Phys. Chem. Lett.* **2016**, *7*, 2346–2349. [CrossRef] [PubMed]
48. Lin, W.; Chen, G.-J.J.; Sun, C.-Y.Y.; Guo, X.-Q.Q.; Wu, Z.-K.K.; Liang, M.-Y.Y.; Chen, L.-T.T.; Yang, L.-Y.Y. Effect of surfactant on the formation and dissociation kinetic behavior of methane hydrate. *Chem. Eng. Sci.* **2004**, *59*, 4449–4455. [CrossRef]
49. Pandey, J.S.; Almenningen, S.; von Solms, N.; Ersland, G. Pore-Scale Visualization of CH$_4$ Gas Hydrate Dissociation under Permafrost Conditions. *Energy Fuels* **2021**, *35*, 1178–1196. [CrossRef]
50. Sato, H.; Tsuji, T.; Nakamura, T.; Uesugi, K.; Kinoshita, T.; Takahashi, M.; Mimachi, H.; Iwasaki, T.; Ohgaki, K. Preservation of Methane Hydrates Prepared from Dilute Electrolyte Solutions. *Int. J. Chem. Eng.* **2009**, *2009*, 843274. [CrossRef]
51. Sato, H.; Sakamoto, H.; Ogino, S.; Mimachi, H.; Kinoshita, T.; Iwasaki, T.; Sano, K.; Ohgaki, K. Self-preservation of methane hydrate revealed immediately below the eutectic temperature of the mother electrolyte solution. *Chem. Eng. Sci.* **2013**, *91*, 86–89. [CrossRef]

52. Mimachi, H.; Takeya, S.; Gotoh, Y.; Yoneyama, A.; Hyodo, K.; Takeda, T.; Murayama, T. Dissociation behaviors of methane hydrate formed from NaCl solutions. *Fluid Phase Equilib.* **2016**, *413*, 22–27. [CrossRef]

53. Chen, X.; Li, S.; Zhang, P.; Chen, W.; Wu, Q.; Zhan, J.; Wang, Y. Promoted Disappearance of CO2 Hydrate Self-Preservation Effect by Surfactant SDS. *Energies* **2021**, *14*, 3909. [CrossRef]

54. Zhang, G.; Rogers, R.E. Ultra-stability of gas hydrates at 1atm and 268.2K. *Chem. Eng. Sci.* **2008**, *63*, 2066–2074. [CrossRef]

55. Takeya, S.; Ripmeester, J.A. Dissociation behavior of clathrate hydrates to ice and dependence on guest molecules. *Angew. Chem. Int. Ed.* **2008**, *47*, 1276–1279. [CrossRef]

56. Ohno, H.; Narita, H.; Nagao, J. Different Modes of Gas Hydrate Dissociation to Ice Observed by Microfocus X-ray Computed Tomography. *J. Phys. Chem. Lett.* **2011**, *2*, 201–205. [CrossRef]

57. Giavarini, C.; Maccioni, F. Self-Preservation at Low Pressures of Methane Hydrates with Various Gas Contents. *Ind. Eng. Chem. Res.* **2004**, *43*, 6616–6621. [CrossRef]

58. Stern, L.A.; Circone, S.; Kirby, S.H.; Durham, W.B. Temperature, pressure, and compositional effects on anomalous or "self" preservation of gas hydrates. *Can. J. Phys.* **2003**, *81*, 271–283. [CrossRef]

59. Circone, S.; Stern, L.A.; Kirby, S.H. The effect of elevated methane pressure on methane hydrate dissociation. *Am. Mineral.* **2004**, *89*, 1192–1201. [CrossRef]

60. Falenty, A.; Kuhs, W.F.; Glockzin, M.; Rehder, G. "self-preservation" of CH4 hydrates for gas transport technology: Pressure-temperature dependence and ice microstructures. *Energy Fuels* **2014**, *28*, 6275–6283. [CrossRef]

61. Zhang, L.; Dong, H.; Dai, S.; Kuang, Y.; Yang, L.; Wang, J.; Zhao, J.; Song, Y. Effects of depressurization on gas production and water performance from excess-gas and excess-water methane hydrate accumulations. *Chem. Eng. J.* **2022**, *431*, 133223. [CrossRef]

62. Takeya, S.; Uchida, T.; Nagao, J.; Ohmura, R.; Shimada, W.; Kamata, Y.; Ebinuma, T.; Narita, H. Particle size effect of CH4 hydrate for self-preservation. *Chem. Eng. Sci.* **2005**, *60*, 1383–1387. [CrossRef]

63. Seo, Y.T.; Moudrakovski, I.L.; Ripmeester, J.A.; Lee, J.W.; Lee, H. Efficient recovery of CO2 from flue gas by clathrate hydrate formation in porous silica gels. *Environ. Sci. Technol.* **2005**, *39*, 2315–2319. [CrossRef]

64. Shanker Pandey, J.; Jouljamal Daas, Y.; Paul Karcz, A.; Solms, N. Von Methane Hydrate Formation Behavior in the Presence of Selected Amino Acids. *J. Phys. Conf. Ser.* **2020**, *1580*, 012003. [CrossRef]

65. Li, G.; Wu, D.; Li, X.; Zhang, Y.; Lv, Q.; Wang, Y. Experimental Investigation into the Production Behavior of Methane Hydrate under Methanol Injection in Quartz Sand. *Energy Fuels* **2017**, *31*, 5411–5418. [CrossRef]

66. Sira, J.H.; Patil, S.L.; Kamath, V.A. Study of Hydrate Dissociation by Methanol and Glycol Injection. In Proceedings of the SPE Annual Technical Conference and Exhibition, New Orleans, LA, USA, 23 September 1990; pp. 977–984.